

# Muon Momentum Scale using $Z \rightarrow \mu\mu$ Sample

Arie Bodek, Willis Sakumoto, and Jiyeon Han

*University of Rochester, Rochester NY, USA*

## Abstract

We report on the muon momentum scale study using Drell-Yan  $\mu^+\mu^-$  pairs in the  $Z$  Mass Region ( $60 < M_{ee} < 120 \text{ GeV}/c^2$ ) from  $pp$  Collisions at  $\sqrt{s}=7 \text{ TeV}$ . The data sample used for the study corresponds to  $2.1 \text{ fb}^{-1}$  of integrated luminosity collected until August, 22nd (2011A data set). The muon momentum scale is applied to correct  $\eta$  and  $\phi$  dependence which is caused by the misalignment of the detector.

Version 1

# 1 Introduction

We report on the muon momentum scale study using Drell-Yan  $\mu^+\mu^-$  pairs in the  $Z$  Mass Region ( $60 < M_{ee} < 120 \text{ GeV}/c^2$ ) from  $pp$  Collisions at  $\sqrt{s}=7 \text{ TeV}$ .

The CMS reconstruction software has an incorrect alignment geometry of the tracker. This affects the momentum determination of muons. The misalignment of the tracker results in a charge ( $Q$ ),  $\eta$ , and  $\phi$  dependence of the determination of the muon momentum. To resolve this problem, the data set is reproduced using the latest alignment geometry, but the misalignment of the tracker still remains. To correct the remaining misalignment effect, the CMS official momentum correction (MuscleFit) is developed by the tracking group. This correction is described using the Ansatz function. The Ansatz functions that are used to correct for the residual charge,  $\eta$ , and  $\phi$  dependence of the determination of the muon momentum and the functional forms are different for data and MC. The MuscleFit correction is updated up to  $750 \text{ pb}^{-1}$  for 2011 data (not approved yet) [1], but not available for 2011 MC set. It uses the parameterization of the functional form, so it is more complicated. Here, we develop the muon momentum scale which has the charge,  $\eta$ , and  $\phi$  dependence using the average of  $1/p_T$  ( $< 1/p_T >$ ).

## 2 Data Set and Event Selection

For the muon momentum study, we use 2011A data set corresponding to  $2.1 \text{ fb}^{-1}$  of integrated luminosity passing HLT DoubleMu\_7 trigger path. It is reproduced in CMSSW\_4\_2\_8 version. The Jason file is required to select the runs which has a good detector condition. The MC set is  $Z \rightarrow \mu\mu$  Powheg sample of Summer 11 version which includes Pythia parton showering. The selection of the analysis is same as the Vector Boson Task Force outlined in: <https://twiki.cern.ch/twiki/bin/viewauth/CMS/VbtfZMuMuBaselineSelection>. In the definition of isolation, we use the combined track and HCAL fractional isolation  $(TrkIso + HadIso)_{\Delta R < 0.3}/P_T < 0.15$  (as used by the Dilepton group). If the EM energy is not included in the isolation requirement, then the the momentum dependence of the efficiency is expected to be constant. If the EM energy is included in the isolation requirement, than the FSR photons would result in a momentum dependence and a more complicated correlation between the efficiency of the two muons. Specifically, the selection criteria are:

- HLT DoubleMu\_7
- Muon selection : VBTF muon selection is applied
- $P_t > 20 \text{ GeV}$  and detector  $|\eta| < 2.4$
- Global and Tracker Muon
- Combined relative isolation :  $(TrkIso + HadIso)_{\Delta R < 0.3}/P_T < 0.15$
- Global muon normalized fit  $\chi^2 < 10$
- Number of Tracker hits greater than 10
- Number of pixel hits greater than or equal to 1
- Number of muon stations greater than or equal to 2
- $dxy < 0.2$
- Mass selection :  $60 < Mass < 120 \text{ GeV}/c^2$

The muon reconstruction efficiency is estimated using data as a function of  $\eta$  and the efficiency scale factor of data to MC is applied into MC to correct the difference of the efficiency between the data and MC.

## 3 Reference Plot of Muon Momentum Study

The misalignment of the tracker generates several effects in the kinematic distribution of Drell-Yan ( $Z/\gamma^* \rightarrow \mu\mu$ ) events. It produces the charge,  $\eta$ , and  $\phi$  dependence of  $Z$  mass, and also the difference of overall  $Z$  mass distribution between the data and MC because the data and MC has the different misalignment scenario. The charge dependence of muon momentum also creates the unexpected wiggles around  $Z$  peak region in the forward and backward asymmetry ( $A_{fb}$ ). In low  $Z$  boson  $P_T$  region ( $P_T < 10 \text{ GeV}/c$ ),  $\phi$  distribution in Collins-Soper

55 frame (CS) [3],  $\phi_{CS}$ , is expected to be flat. However, the muon momentum resolution smearing in the reconstructed  
 56 level generates the excess around  $\phi_{CS} = 0$  and  $\pm\pi$ . The level of the excess at  $\phi_{CS} = 0$  and  $\pm\pi$  is expected to be  
 57 same if the muon momentum scale and resolution is same between  $\mu^+$  and  $\mu^-$ . Therefore,  $\phi_{CS}$  distribution in low  
 58  $Z P_T$  region provides an additional indication of the muon momentum scale study.

59 For the muon momentum study, these kinematic distributions, the dimuon invariant mass ( $M_{\mu^+\mu^-}$ ),  $A_{fb}$ , and  $\phi_{CS}$   
 60 in  $Z P_T < 10 \text{ GeV}/c$ , are used as the reference plot of the study. Figure 1 and 2 show the reference plots before  
 61 any muon momentum correction.

## 62 4 Muon Momentum Correction

63 To resolve the misalignment of the track, we apply the muon momentum correction in charge (Q),  $\eta$ , and  $\phi$  of the  
 64 muon. We estimate the average of  $1/p_T$  ( $< 1/p_T >$ ) in data and MC in Q,  $\eta$ , and  $\phi$  of the muon. The  $< 1/p_T >$   
 65 of the data and MC (reconstructed level) is tuned to be the  $< 1/p_T >$  of the generated level in MC. The correction  
 66 factor is obtained by the  $< 1/p_T >$  difference of data or MC (reconstructed level) to MC (generated level). Figure  
 67 3 shows the  $< 1/p_T >$  correction of data and MC ( $C^{Data/MC}(Q, \eta, \phi)$ ). The correction is applied into the data  
 68 and MC in the additive way.

$$C^{Data/MC}(Q, \eta, \phi) = \langle 1/p_T^{Data/MC(rec.)}(Q, \eta, \phi) \rangle - \langle 1/p_T^{MC(gen.)}(Q, \eta, \phi) \rangle \quad (1)$$

$$\frac{1}{p_T^{corrected}} = \frac{1}{p_T} - C^{Data/MC}(Q, \eta, \phi) \Leftrightarrow p_i^{corrected} = p_i \times \frac{1.0}{1.0 - p_T * C^{Data/MC}(Q, \eta, \phi)} \quad (2)$$

69 where  $C^{Data/MC}$  is the correction factor for the data or MC in Q,  $\eta$ , and  $\phi$  of the muon ( $8 \times 8$  matrix for  $\eta$  and  
 70  $\phi$ ), MC(rec.) and MC(gen.) is the information of MC in the reconstructed and generated level, and  $p_i$  is the  
 71 momentum of the muon in  $x$ ,  $y$ , and  $z$  direction ( $i = x, y, z$ ). This  $< 1/p_T >$  correction fixes the charge,  $\eta$ , and  
 72  $\phi$  dependence of the momentum.

73 After applying the  $< 1/p_T >$  correction, we apply the global factors to match MC to the data for the Z mass and  
 74 resolution. The three global factors, T,  $\Delta$ , and SF, are estimated by comparing  $M_{\mu^+\mu^-}$  distribution between the  
 75 data and MC ( $\chi^2$  test). Figure 4 shows  $\chi^2$  distribution as a function of the global factors. The measured global  
 76 factors from  $\chi^2$  test are summarized in Table 1.

$$p_i^{corrected} = p_i + T \times (p_i^{gen.} - p_i) \quad (3)$$

$$\frac{1}{p_T^{corrected}} = \frac{1}{p_T} + \Delta \times \text{Random} :: \text{Gaus}(1, SF) \quad (4)$$

77 where  $p_i$  is the reconstructed muon momentum in MC ( $i = x, y, \text{ and } z$ ) and  $p_i^{gen.}$  is the generated muon momentum  
 78 in MC.

Table 1: The global factors (T,  $\Delta$ , and SF) of the muon momentum correction. The global factors are estimate  
 comparing  $M_{\mu^+\mu^-}$  distribution. These factors are applied into MC.

Global Factor	Value
T	$0.9433 \pm 0.0020$
$\Delta$	$(2.2541 \pm 0.0792) \times 10^{-5}$
SF	$10.3708 \pm 0.3708$

79 After applying the correction factors,  $C(Q, \eta, \phi)$ , T,  $\Delta$ , and SF, the reference plots shows better agreement between  
 80 the data and MC and also the reasonable feature in  $A_{fb}$  and  $\phi_{CS}$  distribution. The  $\phi_{CS}$  distributions in low Z  
 81  $P_T$  region shown in Figure 5 show the offset between the data and MC because of the normalization effect. (The

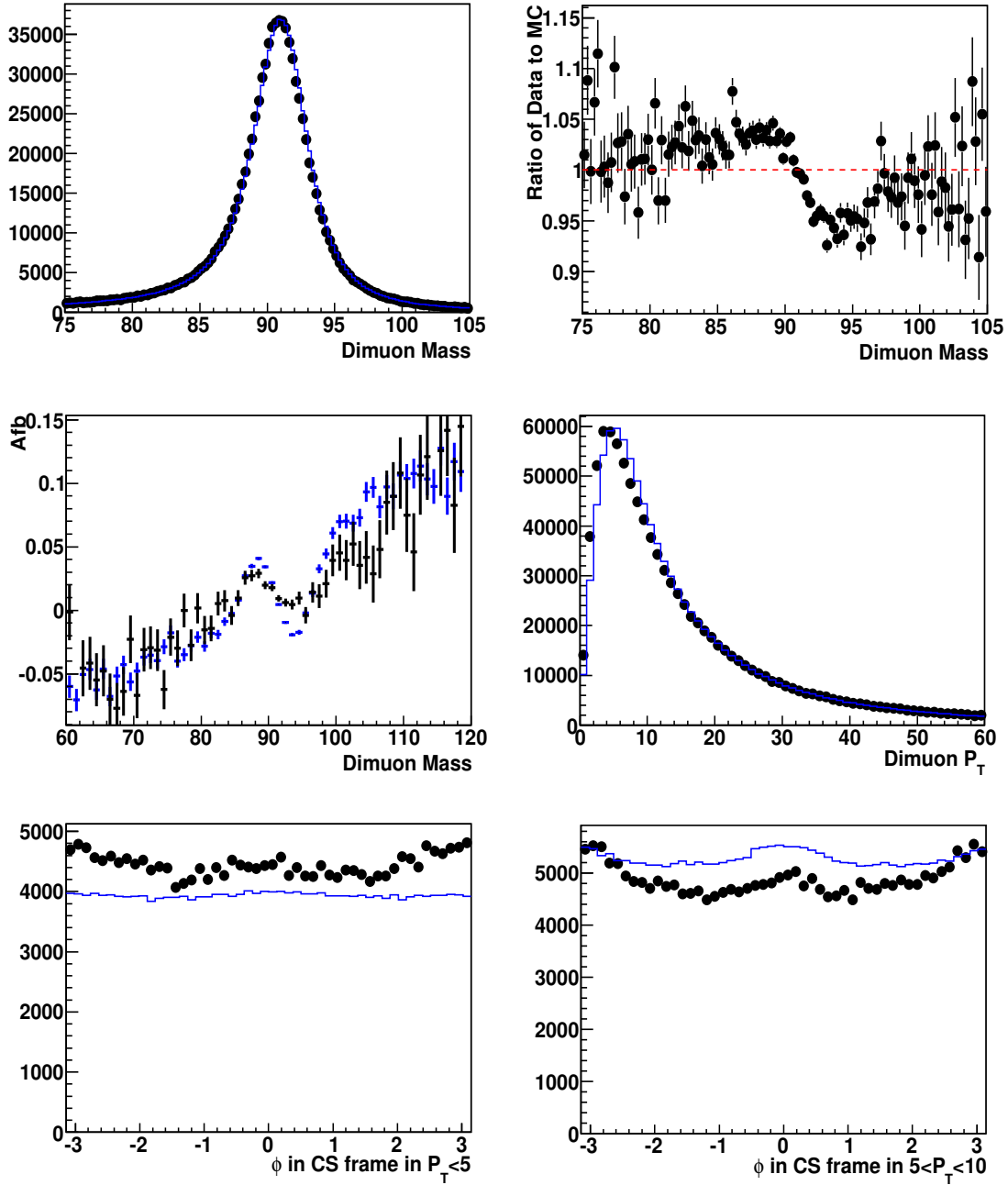


Figure 1: Top Plots: Comparison of the dimuon invariant mass distribution between the data (black) and MC (blue) (left) and its ratio of data to MC (right). Middle plots: Comparison of  $A_{fb}$  (left) and boson  $P_T$  (right) distributions between the data (black) and MC (blue). Bottom plots: Comparison of  $\phi$  in the Collins-Soper frame in boson  $P_T < 5 \text{ GeV}/c$  (left) and  $\phi$  in the Collins-Soper frame in boson  $5 < P_T < 10 \text{ GeV}/c$  (right) distributions between the data (black) and MC (blue). The plots are normalized to the total number of events of the data in  $60 < M_{\mu\mu} < 120 \text{ GeV}/c^2$ .

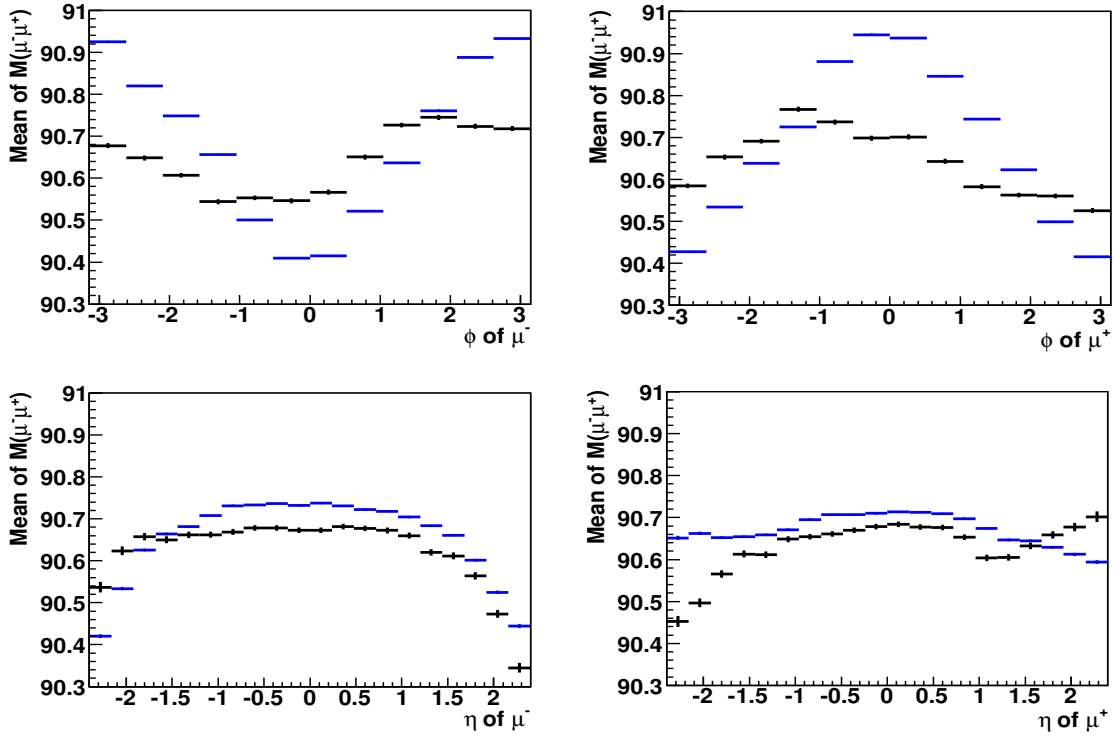


Figure 2: Top Plots: Comparison of the average of  $M_{\mu\mu}$  in  $\phi$  of  $\mu^-$  (left) and the average of  $M_{\mu\mu}$  in  $\phi$  of  $\mu^+$  (right) between the data (black) and MC (blue). Bottom Plots: Comparison of the average of  $M_{\mu\mu}$  in  $\eta$  of  $\mu^-$  (left) and the average of  $M_{\mu\mu}$  in  $\eta$  of  $\mu^+$  (right) between the data (black) and MC (blue).

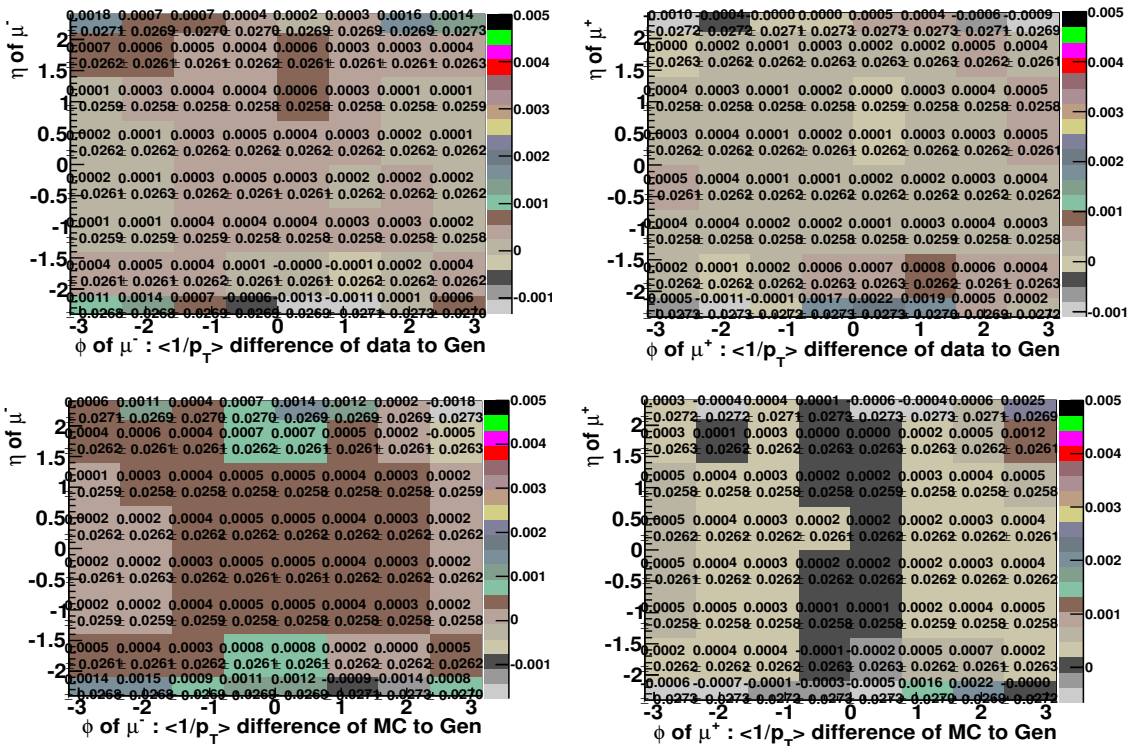


Figure 3: Top Plots: The  $\langle 1/p_T \rangle$  correction of the data for  $\mu^-$  (left) and  $\mu^+$  (right) in  $\eta$  and  $\phi$ . Bottom Plots: The  $\langle 1/p_T \rangle$  correction of the data for  $\mu^-$  (left) and  $\mu^+$  (right) in  $\eta$  and  $\phi$ .

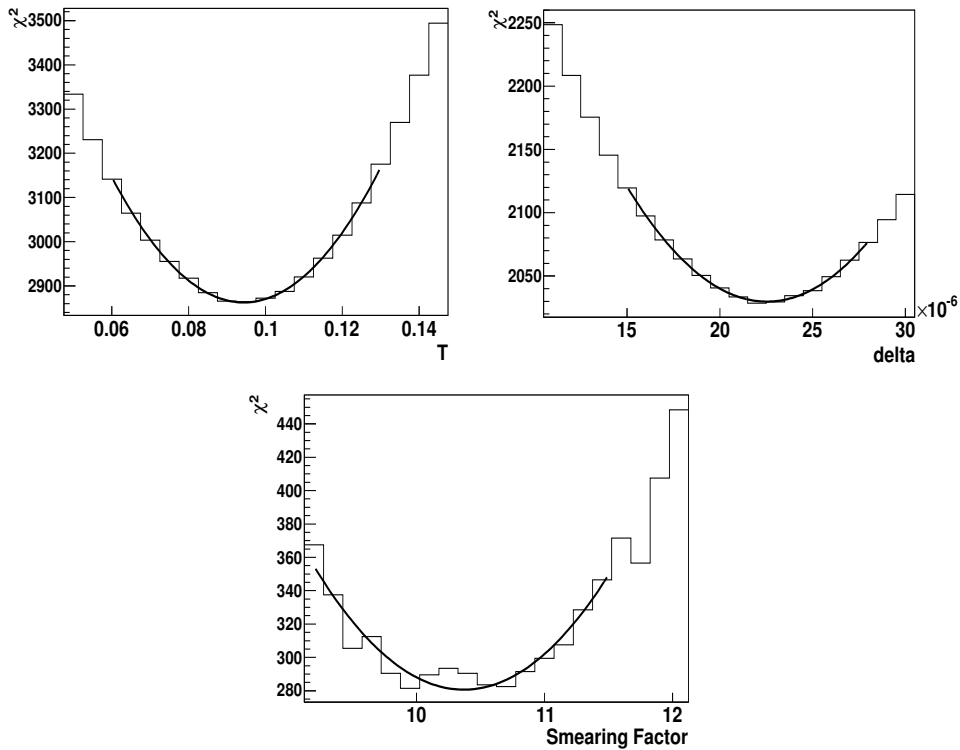


Figure 4: Top Plots:  $\chi^2$  distribution as a function of the global factor, T (left) and  $\Delta$  (right). Bottom Plots:  $\chi^2$  distribution as a function of the global factor, SF.

82 distributions are normalized to the total number of events in data with  $60 < M_{\mu^+\mu^-} < 120 \text{ GeV}/c^2$  mass window.)  
 83 Figure 5 and 6 show the reference plots after applying the muon momentum correction.

84 The Powheg generator with Pythia parton showering has shown the reasonable agreement with the data so far, but  
 85 is not perfect. Especially, Z boson  $P_T$  spectrum in low  $P_T$  region is not described by Powheg generator. [5] For the  
 86 better comparison between data and MC, we apply Z  $P_T$  correction into MC to describe the data. Since the  $\phi_{CS}$   
 87 distribution has Z  $P_T$  dependence, the Z  $P_T$  correction removes the bias in the comparison of  $\phi_{CS}$  distribution  
 88 between the data and MC for the muon momentum study. Figure 7 shows the reference plots after applying the  
 89 additional Z  $P_T$  correction in MC. After the additional Z  $P_T$  correction,  $\phi_{CS}$  has the better matches between the  
 90 data and MC.

## 91 5 Conclusion

92 We report the muon momentum correction to resolve the misalignment of the track. The correction is obtained  
 93 using  $\langle 1/p_T \rangle$  of the muon in the charge,  $\eta$ , and  $\phi$  and the di-muon invariant mass distribution. The muon  
 94 momentum correction removes the bias from the charge (Q),  $\eta$ , and  $\phi$  of the muon. The reference plots,  $M_{\mu^+\mu^-}$ ,  
 95  $A_{fb}$ ,  $\phi_{CS}$  distributions, are used to confirm how the muon momentum correction works well. After the muon  
 96 momentum correction, the bias of charge,  $\eta$ , and  $\phi$  dependence gets removed and all kinematic distributions have  
 97 a good agreement between the data and MC. The muon momentum correction will be provided to apply in the  
 98 offline code.

## 99 6 Appendix

### 100 6.1 MuscleFit Effect

101 The MuscleFit correction is the standard method to correct the muon momentum bias. The MuscleFit correction  
 102 is not available for full 2011 data set yet. However, MuscleFit is updated up to  $750 \text{ pb}^{-1}$  for 2011A data set [1]  
 103 and we test how well MuscleFit works to resolve the muon momentum bias. MuscleFit for MC (2011 Spring  
 104 version) is not available, so we apply MuscleFit of 2010 MC version. To test the MuscleFit effect, we use the

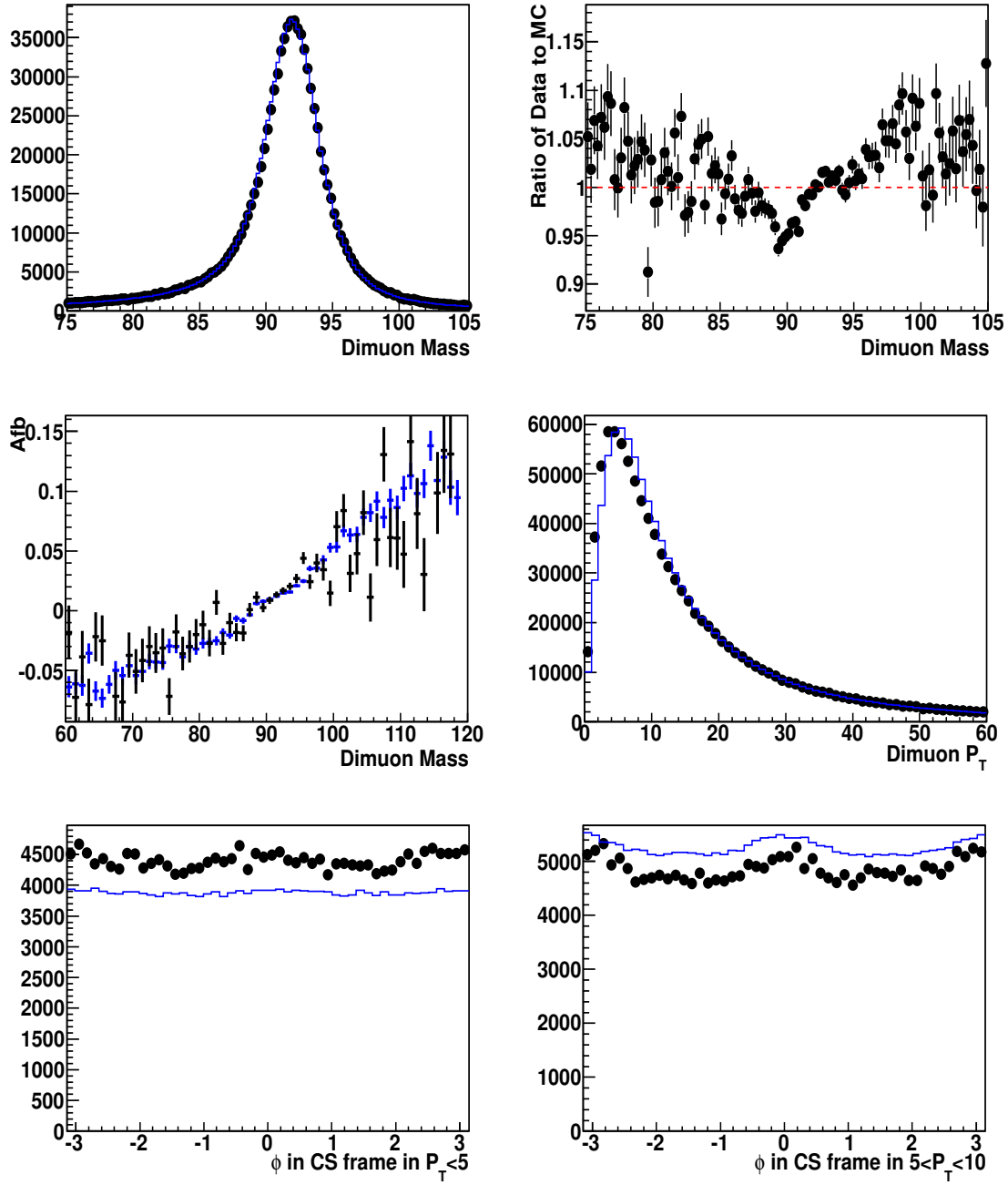


Figure 5: The reference plots ( $M_{\mu^+\mu^-}$ ,  $A_{fb}$ ,  $Z P_T$ , and  $\phi_{CS}$ ) after muon momentum correction. Top Plots: Comparison of the dimuon invariant mass distribution between the data (black) and MC (blue) (left) and its ratio of data to MC (right). Middle plots: Comparison of  $A_{fb}$  (left) and boson  $P_T$  (right) distributions between the data (black) and MC (blue). Bottom plots: Comparison of  $\phi$  in the Collins-Soper frame in boson  $P_T < 5$  GeV/c (left) and  $\phi$  in the Collins-Soper frame in boson  $5 < P_T < 10$  GeV/c (right) distributions between the data (black) and MC (blue). The plots are normalized to the total number of events of the data in  $60 < M_{\mu\mu} < 120$  GeV/c<sup>2</sup>.

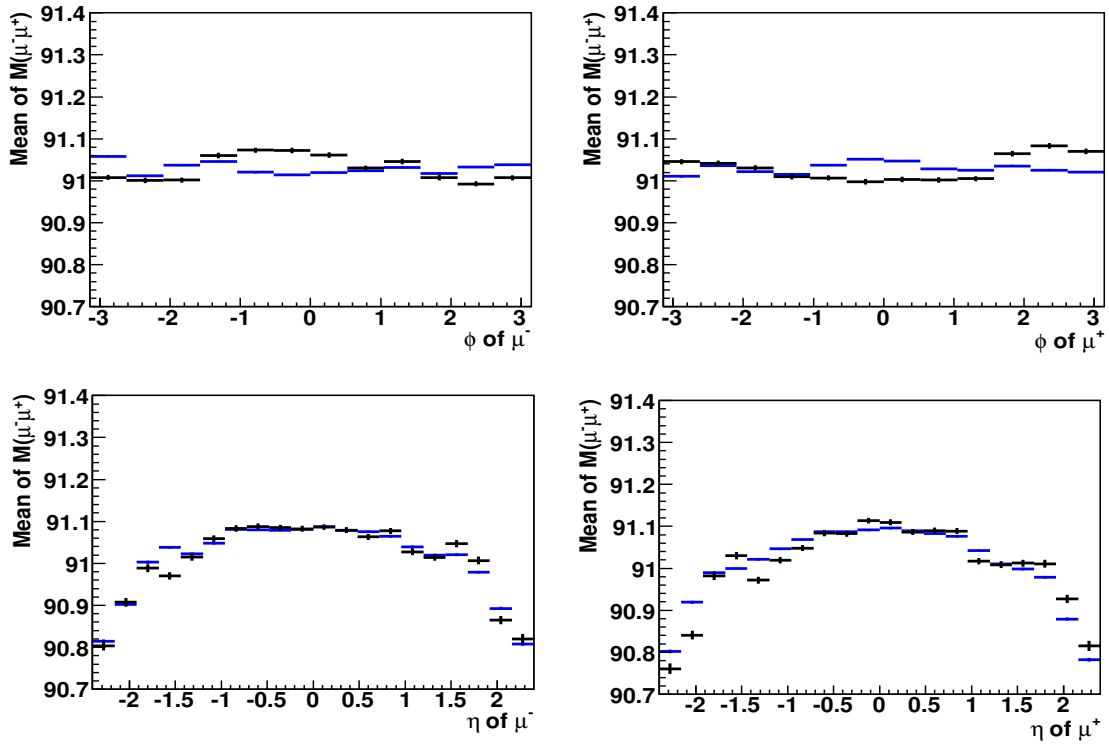


Figure 6: The  $M_{\mu^+\mu^-}$  profile plot as a function of  $\eta$  and  $\phi$  of  $\mu^+$  and  $\mu^-$  after the muon momentum correction. Top Plots: Comparison of the average of  $M_{\mu\mu}$  in  $\phi$  of  $\mu^-$  (left) and the average of  $M_{\mu\mu}$  in  $\phi$  of  $\mu^+$  (right) between the data (black) and MC (blue). Bottom Plots: Comparison of the average of  $M_{\mu\mu}$  in  $\eta$  of  $\mu^-$  (left) and the average of  $M_{\mu\mu}$  in  $\eta$  of  $\mu^+$  (right) between the data (black) and MC (blue).

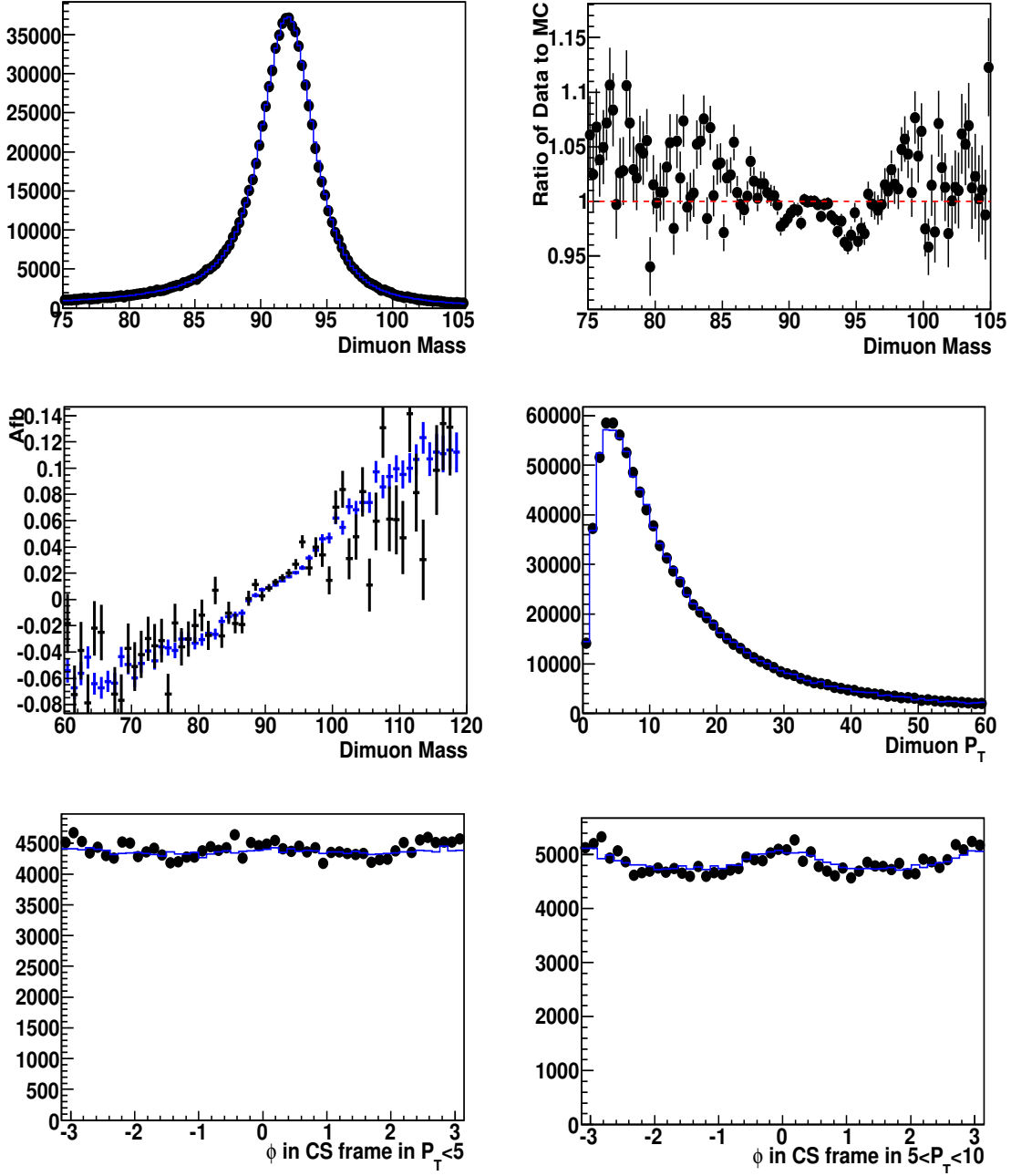


Figure 7: The reference plots ( $M_{\mu^+\mu^-}$ ,  $A_{fb}$ ,  $Z P_T$ , and  $\phi_{CS}$ ) after muon momentum correction and  $Z P_T$  correction. Top Plots: Comparison of the dimuon invariant mass distribution between the data (black) and MC (blue) (left) and its ratio of data to MC (right). Middle plots: Comparison of  $A_{fb}$  (left) and boson  $P_T$  (right) distributions between the data (black) and MC (blue). Bottom plots: Comparison of  $\phi$  in the Collins-Soper frame in boson  $P_T < 5$  GeV/c (left) and  $\phi$  in the Collins-Soper frame in boson  $5 < P_T < 10$  GeV/c (right) distributions between the data (black) and MC (blue). The plots are normalized to the total number of events of the data in  $60 < M_{\mu\mu} < 120$  GeV/c<sup>2</sup>.

105 reference plots which are described in Sec. 3. Figure 8 and 9 show the reference plots of the data and Figure 10  
 106 and 11 show the reference plots of MC before (black) and after (blue) applying MuscleFit. MuscleFit in the data  
 107 improves  $\phi$  dependence of the muon momentum, but does not change other kinematic distributions. MuscleFit  
 108 in MC shifts the mass distribution by  $\sim 0.1 \text{ GeV}/c^2$  and overcorrects  $\phi$  dependence of the muon momentum.  
 109 MC (2010 November version) has the different alignment scenario from MC (2011 Spring version). Therefore,  
 110 MuscleFit for 2010 November version of MC might not work for 2011 Spring version of MC.

111 From the study, MuscleFit improves  $\phi$  dependence of the muon momentum, but cannot improve other bias like the  
 112 effect on  $A_{fb}$ ,  $\phi_{CS}$  distribution, or  $\eta$  dependence. However, MuscleFit used for the study is estimated using the  
 113 part of 2011 data set, so need to confirm the effect using the updated MuscleFit parameters for full data set.

## 114 6.2 Application of $C(Q, \eta, \phi)$ Factor in Multiplicative Way

115 The muon momentum bias can be caused by misalignment of the track or the magnetic field difference. The  
 116 misalignment of the track adds a fixed curvature shift which is equivalent to a fixed shift in  $1/p_T$  and is additive.  
 117 Therefore, a misalignment causes an additive correction and has the opposite sign of the correction for  $\mu^+$  and  $\mu^-$ .  
 118 On the other hands, the magnetic field effect is proportional to  $1/p_T$  and does not have the charge dependence,  
 119 which results in the multiplicative correction.

120 Since the misalignment issue of the track is already known in CMS detector, we estimate the correction factor,  
 121  $C(Q, \eta, \phi)$ , and apply it in the additive way. However, as a part of the study, we also estimate the correction factor  
 122 in the multiplicative way and check the effect in high  $p_T$  region.

123 In the multiplicative way, the correction factor,  $C(Q, \eta, \phi)$ , is estimated by the ratio of  $\langle 1/p_T \rangle^{Data/MC(rec.)}$   
 124 to  $\langle 1/p_T \rangle^{MC(gen.)}$  which is defined as  $C_M(Q, \eta, \phi)$ . The following equations explain how to define and apply  
 125 the correction factor,  $C_M(Q, \eta, \phi)$ .

$$C_M^{Data/MC}(Q, \eta, \phi) = \langle 1/p_T^{Data/MC(rec.)}(Q, \eta, \phi) \rangle / \langle 1/p_T^{MC(gen.)}(Q, \eta, \phi) \rangle \quad (5)$$

$$\frac{1}{p_T^{corrected}} = \frac{1}{p_T} \times C_M^{Data/MC}(Q, \eta, \phi) \Leftrightarrow p_i^{corrected} = \frac{p_i}{C_M^{Data/MC}(Q, \eta, \phi)} \quad (6)$$

126 After applying the multiplicative correction,  $C_M(Q, \eta, \phi)$ , the global factors, T,  $\Delta$ , and SF are estimated using  
 127  $M_{\mu^+\mu^-}$  distribution and these global factors are applied into MC. The reference plots in Z mass region ( $60 <$   
 128  $M_{\mu^+\mu^-} < 120 \text{ GeV}/c^2$ ) with the multiplicative correction shown in Figure 12 are close to the reference plots  
 129 with the additive correction.

130 The multiplicative correction and the additive correction are expected to show the similar effect in Z mass region.  
 131 However, if the muon has very high momentum like  $p_T = 500 \text{ GeV}$ , then the effect is significant different.  
 132 For example, if  $C_M(Q, \eta, \phi) = 0.01$  in the multiplicative way, it changes the momentum with  $p_T^\mu = 50 \text{ GeV}$   
 133 by 1% ( $0.5 \text{ GeV}$ ) and also the momentum with  $p_T^\mu = 500 \text{ GeV}$  by 1% ( $5 \text{ GeV}$ ). In the additive way, if  
 134  $C(Q, \eta, \phi) = 0.0002$ , then it changes the momentum with  $p_T^\mu = 50 \text{ GeV}$  by 1% ( $0.5 \text{ GeV}$ ), but the momentum  
 135 with  $p_T^\mu = 500 \text{ GeV}$  by 10% ( $50 \text{ GeV}$ ). To test the effect of applying the correction factor (multiplicative  
 136 vs. additive way), we compared the muon  $p_T$  between the reconstructed and the generated level in very high  
 137 mass region ( $M_{\mu^+\mu^-} > 250 \text{ GeV}/c^2$ ) using MC to see which way returns the closer reconstructed momentum  
 138 from the generated momentum. The comparison of the reconstructed muon momentum to the generated muon  
 139 momentum shows that the additive correction gives the closer reconstructed muon momentum from the generated  
 140 muon momentum than the multiplicative correction, which is shown in Figure 13. Figure 14 shows the difference  
 141 of  $\langle 1/p_T(rec.) \rangle$  and  $\langle 1/p_T(gen.) \rangle$  in the Z mass region,  $60 < M_{\mu^+\mu^-} < 120 \text{ GeV}/c^2$ . Even in the Z mass  
 142 region, the additive correction returns closer reconstructed muon momentum from the generated muon momentum.

## 143 References

144 [1] MuscleFit for 2011A data set : Presentation in CMS Muon POG Meeting (July. 11th, 2011). The presentation  
 145 is linked at <https://indico.cern.ch/getFile.py/access?contribId=1&resId=0&materialId=slides&confId=128936>.  
 146

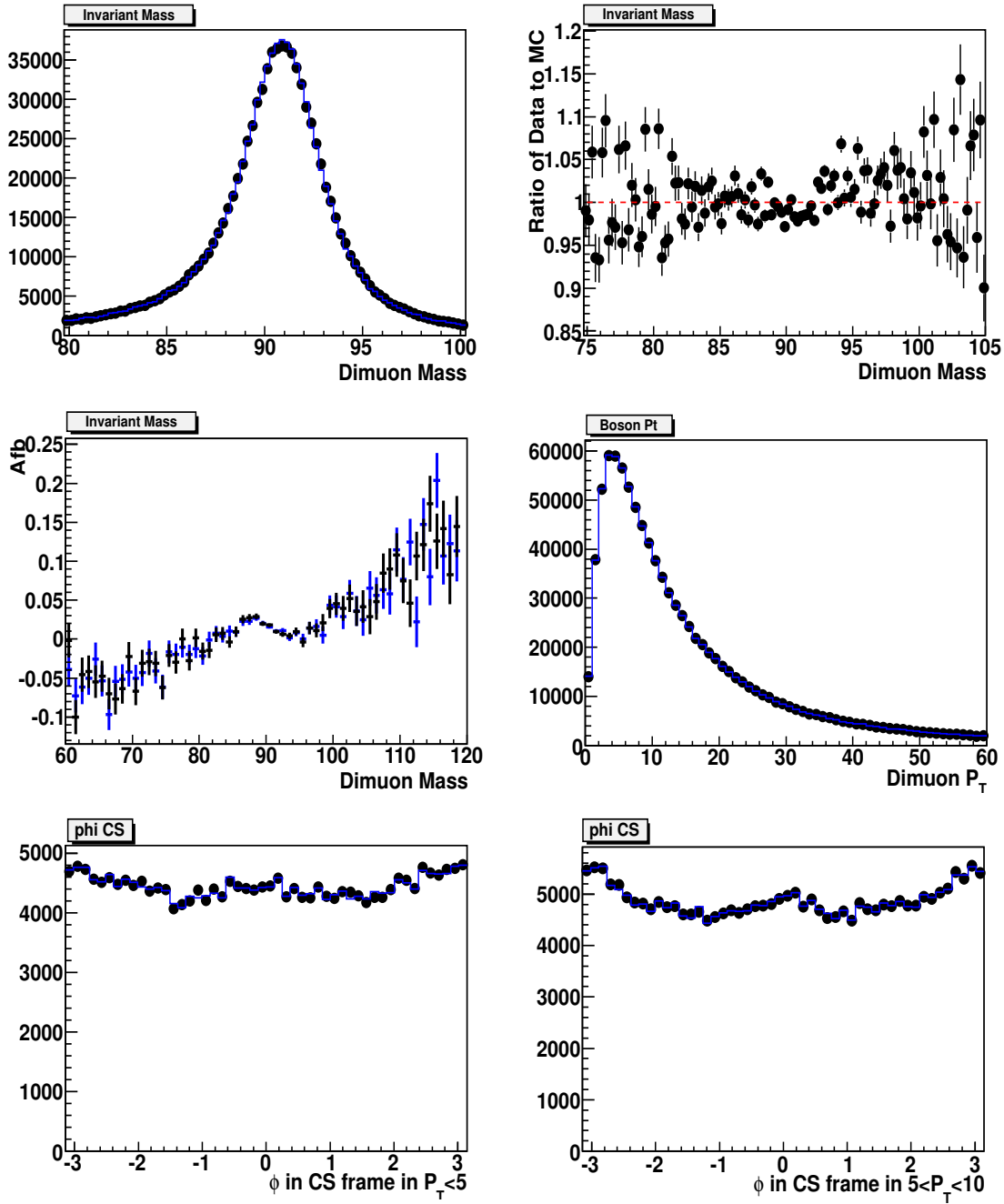


Figure 8: The MuscleFit effect in data. Top Plots: Comparison of the dimuon invariant mass distribution before (black) and after (blue) applying MuscleFit (left) and its ratio (right). Middle plots: Comparison of  $A_{fb}$  (left) and boson  $P_T$  (right) distributions before (black) and after (blue) applying MuscleFit. Bottom plots: Comparison of  $\phi$  in the Collins-Soper frame in boson  $P_T < 5 \text{ GeV}/c$  (left) and  $\phi$  in the Collins-Soper frame in boson  $5 < P_T < 10 \text{ GeV}/c$  (right) distributions before (black) after (blue) applying MuscleFit.

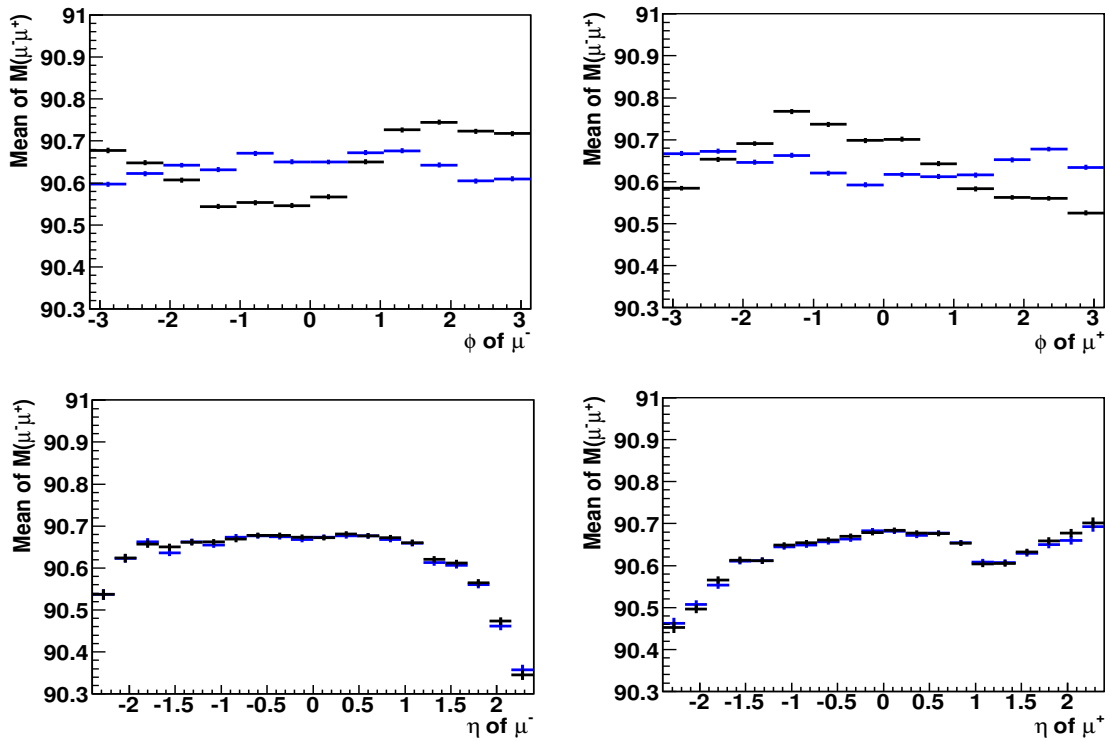


Figure 9: The MuscleFit effect in data. Top Plots: Comparison of the average of  $M_{\mu\mu}$  in  $\phi$  of  $\mu^-$  (left) and the average of  $M_{\mu\mu}$  in  $\phi$  of  $\mu^+$  (right) before (black) and after (blue) applying MuscleFit. Bottom Plots: Comparison of the average of  $M_{\mu\mu}$  in  $\eta$  of  $\mu^-$  (left) and the average of  $M_{\mu\mu}$  in  $\eta$  of  $\mu^+$  (right) before (black) and after (blue) applying MuscleFit.

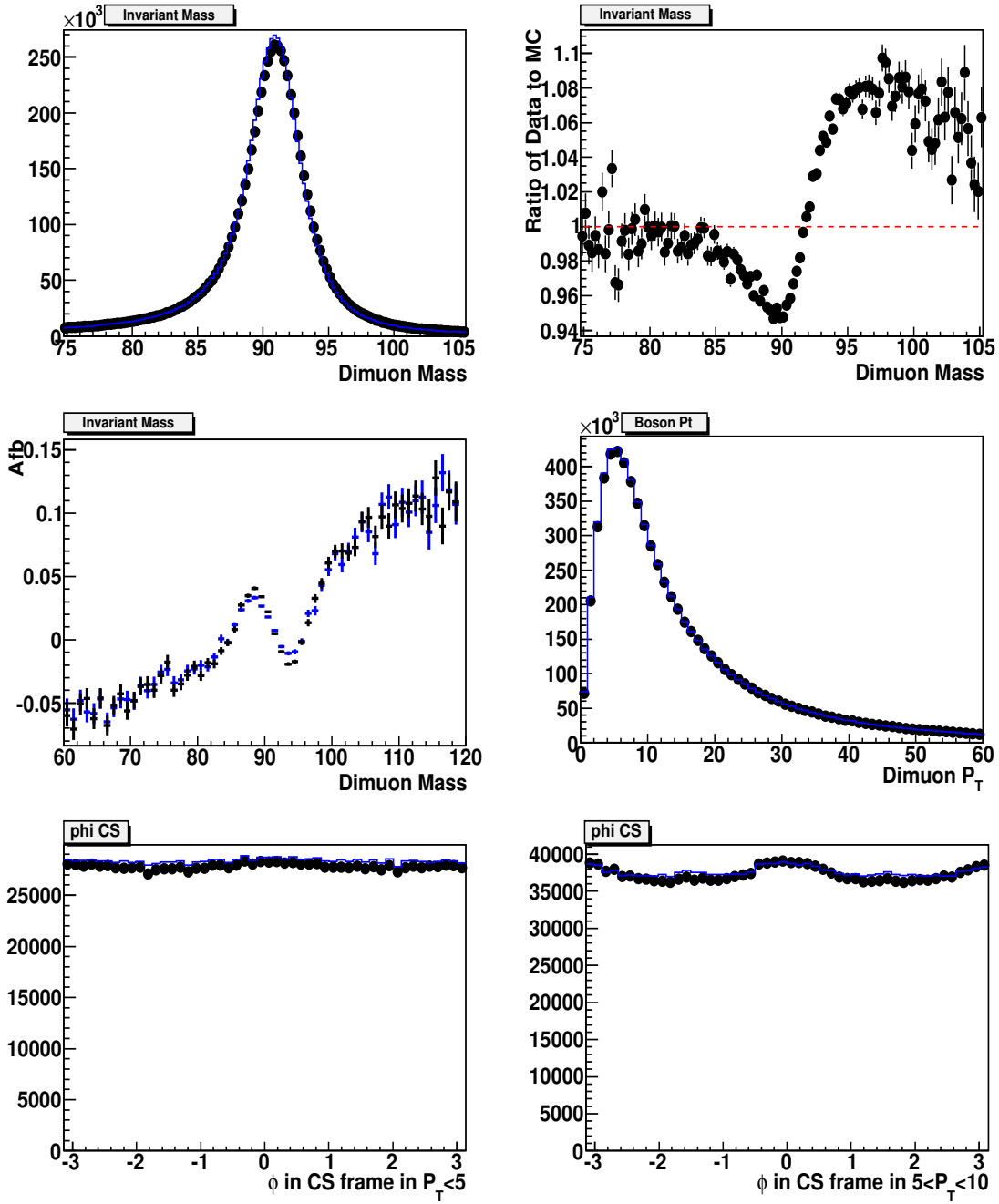


Figure 10: The MuscleFit effect in MC. Top Plots: Comparison of the dimuon invariant mass distribution before (black) and after (blue) applying MuscleFit (left) and its ratio (right). Middle plots: Comparison of  $A_{fb}$  (left) and boson  $P_T$  (right) distributions before (black) and after (blue) applying MuscleFit. Bottom plots: Comparison of  $\phi$  in the Collins-Soper frame in boson  $P_T < 5 \text{ GeV}/c$  (left) and  $\phi$  in the Collins-Soper frame in boson  $5 < P_T < 10 \text{ GeV}/c$  (right) distributions before (black) after (blue) applying MuscleFit.

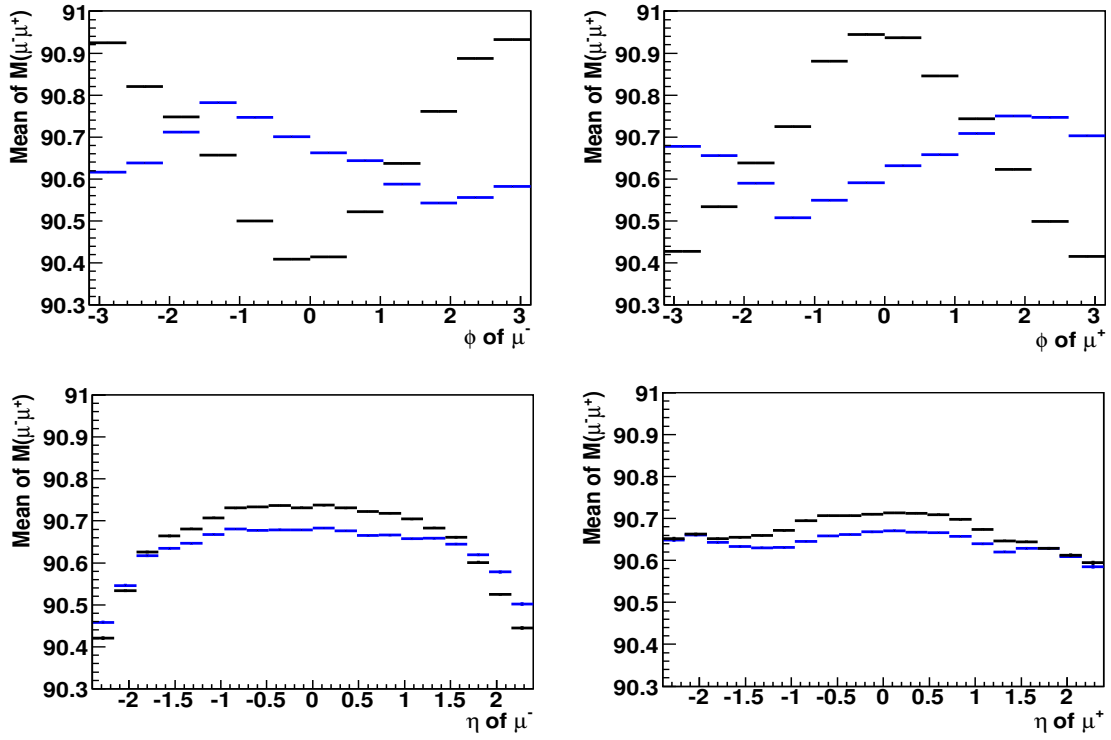


Figure 11: The MuscleFit effect in data. Top Plots: Comparison of the dimuon invariant mass distribution before (black) and after (blue) applying MuscleFit (left) and its ratio (right). Middle plots: Comparison of  $A_{fb}$  (left) and boson  $P_T$  (right) distributions before (black) and after (blue) applying MuscleFit. Bottom plots: Comparison of  $\phi$  in the Collins-Soper frame in boson  $P_T < 5 \text{ GeV}/c$  (left) and  $\phi$  in the Collins-Soper frame in boson  $5 < P_T < 10 \text{ GeV}/c$  (right) distributions before (black) after (blue) applying MuscleFit.

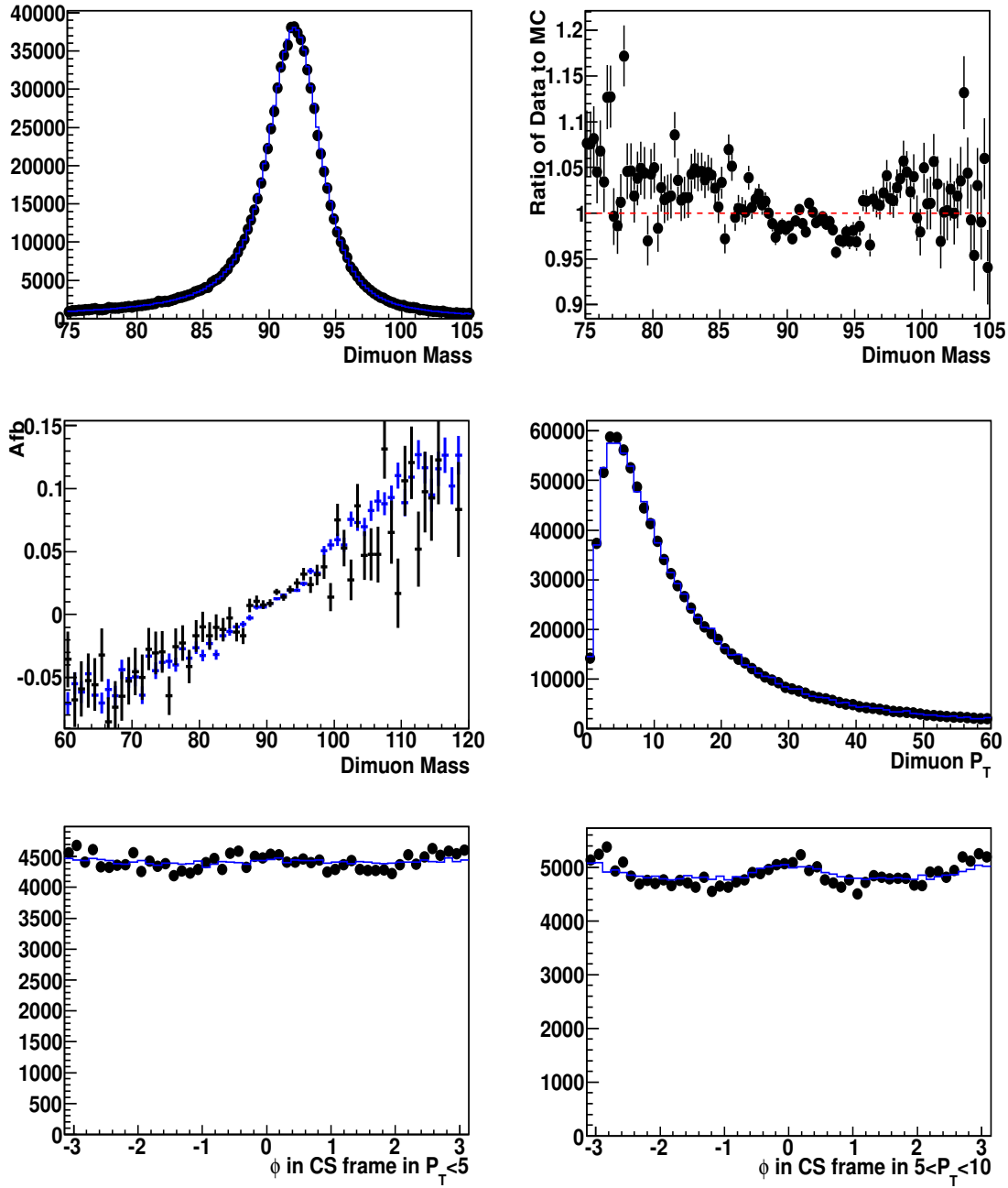


Figure 12: The reference plots ( $M_{\mu^+\mu^-}$ ,  $A_{fb}$ ,  $Z P_T$ , and  $\phi_{CS}$ ) after muon momentum correction in the multiplicative way and  $Z P_T$  correction. Top Plots: Comparison of the dimuon invariant mass distribution between the data (black) and MC (blue) (left) and its ratio of data to MC (right). Middle plots: Comparison of  $A_{fb}$  (left) and boson  $P_T$  (right) distributions between the data (black) and MC (blue). Bottom plots: Comparison of  $\phi$  in the Collins-Soper frame in boson  $P_T < 5 \text{ GeV}/c$  (left) and  $\phi$  in the Collins-Soper frame in boson  $5 < P_T < 10 \text{ GeV}/c$  (right) distributions between the data (black) and MC (blue). The plots are normalized to the total number of events of the data in  $60 < M_{\mu\mu} < 120 \text{ GeV}/c^2$ .

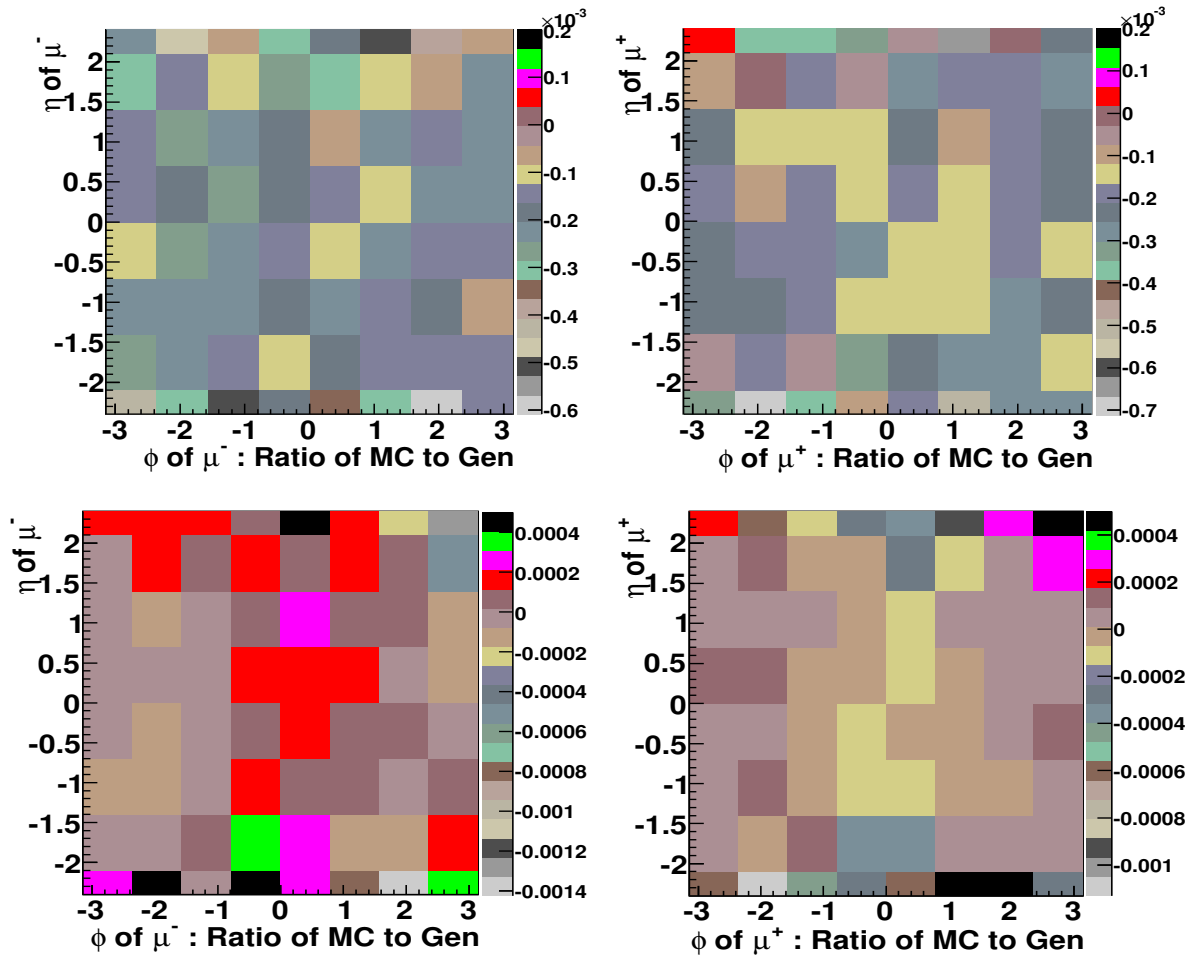


Figure 13: The difference of  $\langle 1/p_T(rec.) \rangle$  and  $\langle 1/p_T(gen.) \rangle$  in  $M_{\mu^+\mu^-} > 250 GeV/c^2$ . Top plot: The difference of  $\langle 1/p_T(rec.) \rangle$  and  $\langle 1/p_T(gen.) \rangle$  after applying the additive correction for  $\mu^-$  (left) and  $\mu^+$  (right). Bottom plot: The difference of  $\langle 1/p_T(rec.) \rangle$  and  $\langle 1/p_T(gen.) \rangle$  after applying the multiplicative correction for  $\mu^-$  (left) and  $\mu^+$  (right).

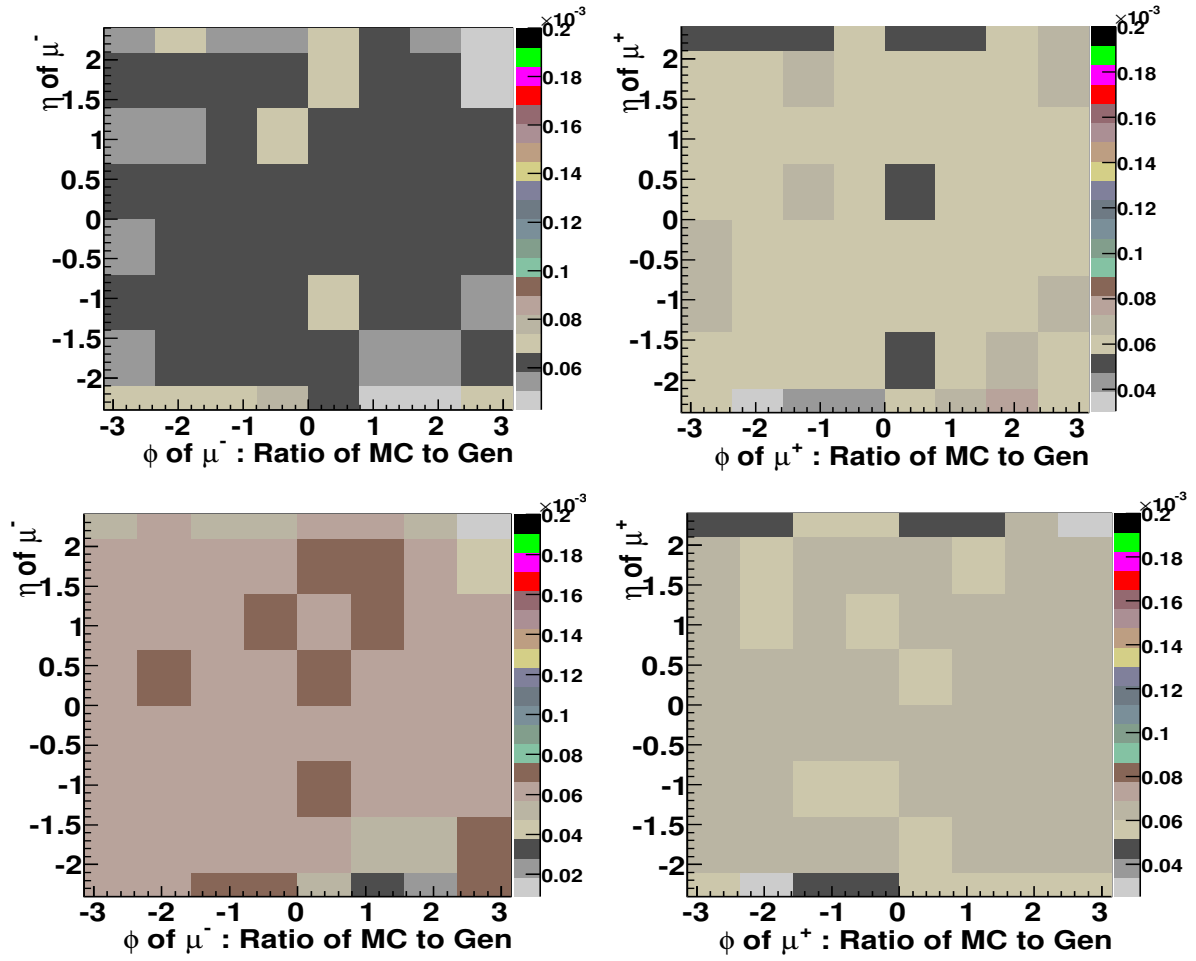


Figure 14: The difference of  $\langle 1/p_T(rec.) \rangle$  and  $\langle 1/p_T(gen.) \rangle$  in  $60 < M_{\mu^+\mu^-} < 120 GeV/c^2$ . Top plot: The difference of  $\langle 1/p_T(rec.) \rangle$  and  $\langle 1/p_T(gen.) \rangle$  after applying the additive correction for  $\mu^-$  (left) and  $\mu^+$  (right). Bottom plot: The difference of  $\langle 1/p_T(rec.) \rangle$  and  $\langle 1/p_T(gen.) \rangle$  after applying the multiplicative correction for  $\mu^-$  (left) and  $\mu^+$  (right).

- 147 [2] For the most recent version of POWHEG. See Simone Alioli , Paolo Nason, Carlo Oleari, Emanuele Re,  
148 arXiv:1009.5594v1 (2010). earlier versions are discussed in JHEP 0807:060,2008. NSF-KITP-08-74, May  
149 2008. 35pp. e-Print: arXiv:0805.4802 [hep-ph]
- 150 [3] J. C. Collins and D. E. Soper, Phys. Rev. D **16**, 2219 (1977). The CS frame is the center of mass of the  $\gamma^*/Z$ ,  
151 where the  $z$  axis is defined as the bisector of the  $p$  and  $\bar{p}$  beams. The polar angle is defined as the angle of the  
152 positive lepton with respect to the proton direction.
- 153 [4] CMS collaboration, “Search for Resonances in the Dimuon Mass Distribution in pp collisions at  $\sqrt{s} = 7$  TeV”,  
154 CMS PAS EXO-10-013 (2010).
- 155 [5] J.G., G.P., D.G., K.K., N.K. (Northeastern University), “Measurement of the  $Z/\gamma^* \rightarrow \mu^+\mu^-$  transverse mo-  
156 mentum distribution in pp collisions at  $\sqrt{s} = 7$  TeV”, CMS note - Archive ID: 30523M